

## Evaluation of “all weather” microwave-derived land surface temperatures with in situ CEOP measurements

J. Catherinot,<sup>1,2</sup> C. Prigent,<sup>2</sup> R. Maurer,<sup>3</sup> F. Papa,<sup>1,4</sup> C. Jiménez,<sup>2</sup> F. Aires,<sup>2,5</sup> and W. B. Rossow<sup>1</sup>

Received 21 June 2011; revised 8 September 2011; accepted 25 September 2011; published 6 December 2011.

[1] Land surface skin temperature  $T_s$  plays a key role in meteorological and climatological processes but the availability and the accuracy of  $T_s$  measurements over land are still limited, especially under cloudy conditions.  $T_s$  estimates from infrared satellite observations can only be derived under clear sky. Passive microwave measurements are much less affected by clouds and can provide  $T_s$  regardless of the cloud conditions. A neural network inversion including first guess information has been previously developed to retrieve  $T_s$ , along with atmospheric water vapor, cloud liquid water, and surface emissivities over land from Special Sensor Microwave/Imager measurements, with a spatial resolution of  $0.25^\circ \times 0.25^\circ$ , at least twice daily. In this study,  $T_s$  estimates are evaluated through careful comparisons with in situ measurements in different environments over a full annual cycle. Under clear sky conditions, the quality of our microwave neural network retrieval is equivalent to the infrared International Satellite Cloud Climatology Project products, for most in situ stations, with errors  $\sim 3$  K as compared to in situ measurements. The performance of the microwave algorithm is similar under clear and cloudy conditions, confirming the potential of the microwaves under clouds. The  $T_s$  accuracy does not depend upon the surface emissivity, as the variability of this parameter is accounted for in the processing. Our microwave  $T_s$  have been calculated for more than 15 years (1993 to mid-2008). These “all weather”  $T_s$  are a very valuable complement to the IR-derived  $T_s$ , for use in atmospheric and surface models.

**Citation:** Catherinot, J., C. Prigent, R. Maurer, F. Papa, C. Jiménez, F. Aires, and W. B. Rossow (2011), Evaluation of “all weather” microwave-derived land surface temperatures with in situ CEOP measurements, *J. Geophys. Res.*, 116, D23105, doi:10.1029/2011JD016439.

### 1. Introduction

[2] Land surface skin temperature ( $T_s$ ) controls and is determined by the balance of radiative heating/cooling and evaporative cooling at the surface. Despite the recognition of its key role in meteorological and climatological processes, accurate  $T_s$  measurements over land areas are not yet available for the whole globe under both clear and cloudy conditions.

[3] Surface skin temperature can be obtained from measurements of infrared radiation at the surface, if the land surface emissivity is known; however, this measurement

is not routinely performed at weather and other research stations. Skin temperatures have been estimated from satellite infrared radiance observations [e.g., Rossow and Garder, 1993; Rossow et al., 1993; Rossow and Schiffer, 1999; Prata, 1993, 1994; Trigo et al., 2008], but direct determinations are possible only under clear sky conditions because clouds block the surface view at these wavelengths.

[4] Several studies have already explored the potential of satellite microwave measurements for land surface temperature retrieval. Microwave wavelengths, being much less affected by water vapor and clouds than infrared, are an attractive alternative especially under cloudy conditions. Note nevertheless that the spatial resolution of passive microwave is much lower than that provided in the infrared (above 10 km with the current microwave radiometers). In addition, passive microwave observations are only available from polar orbiters, contrarily to infrared also observed from geostationary orbits, limiting the time sampling of passive microwave. A few studies correlate the microwave brightness temperature measurements to in situ measurements of near-surface air temperatures made at surface weather stations: since the microwave measurements do not actually sense near-surface air temperature, this approach assumes

<sup>1</sup>NOAA Cooperative Remote Sensing Science and Technology Center, City College of New York, New York, New York, USA.

<sup>2</sup>Laboratoire d'Etudes du Rayonnement et de la Matière en Astrophysique, Observatoire de Paris, CNRS, Paris, France.

<sup>3</sup>NASA Goddard Institute for Space Studies, Columbia University, New York, New York, USA.

<sup>4</sup>Now at Laboratoire d'Etudes en Géophysique et Océanographie Spatiales, IRD, Toulouse, France.

<sup>5</sup>Estellus, Paris, France.

that the surface air and skin temperatures vary together, but this is only approximately true at small spatial and temporal scales and can be badly in error for arid or frozen locations. For instance, *MacFarland et al.* [1990] investigated the correlation between observations from the Special Sensor Microwave /Imager (SSM/I) and "surface air" temperature measurements and used a multivariate regression of the microwave brightness temperatures to retrieve the "surface air" temperature. Later, *Basist et al.* [1998] suggested including the variation of emissivity into account in the regression, using a simple land classification scheme (that algorithm has been evaluated by *Williams et al.* [2000]). *Jones et al.* [2010] also derived a daily estimate of the "surface air" temperature from AMSR-E observations. *Njoku* [1995] concluded from simulations that surface skin temperatures could be estimated from multichannel microwave observations with an accuracy between 2.0 and 2.5 K. A physical retrieval of surface skin temperature using SSM/I observations at 19 and 22 GHz has been developed by *Weng and Grody* [1998]: the two frequencies have approximately the same emissivities so that the emissivity effect on the measurements can be neglected. Note, however, that the actual temperature error is nearly 3 K for every 1% error in surface emissivity at microwave wavelengths. Compared to surface air temperature measurements, the *Weng and Grody* [1998] results exhibited root mean square (r.m.s.) differences of 4.4 K, with a larger bias in colder environments. *Holmes et al.* [2009] proposed a very simple land surface temperature algorithm, based on a single frequency channel (37 GHz in vertical polarization). Other methodologies have been developed for regional studies using algorithms that cannot be directly adopted globally, e.g., the methodology of *Wen et al.* [2003] for over the Tibetan Plateau or of *Royer and Poirier* [2010] for in Boreal North America. *Aires et al.* [2001] developed a global method based on a neural network inversion of a radiative transfer model and ancillary data sets describing the properties of the atmosphere. The scheme retrieves simultaneously over land the surface skin temperature ( $T_s$ ), the atmospheric column water vapor abundance, the cloud liquid water path and the surface emissivities for all SSM/I channels. The algorithm uses pre-calculated monthly-mean emissivities, cloud and surface parameters from infrared and visible satellite information, and the meteorological reanalysis as first guess information. So far, the accuracy of these retrieved surface skin temperatures under cloudy conditions has only been evaluated by comparison with in situ surface air temperature [*Prigent et al.*, 2003a].

[5] In this study, we evaluate the microwave-based  $T_s$  retrieval based on neural network inversion by comparison with in situ  $T_s$  measurements collected during the Coordinated Energy and water cycle Observations Project (CEOP). The comparisons cover diverse environments over a full annual cycle (for 2003). The neural network retrieval method is briefly described, along with the data sets used in the comparison study in Section 2. In section 3, the microwave-derived  $T_s$  estimates are compared to the satellite IR retrievals under clear sky conditions, and then carefully evaluated with respect to the CEOP measurements, under both clear and cloudy conditions. Section 4 summarizes our results and argues for the value of producing merged satellite infrared- and microwave-derived surface skin temperature to better

characterize the energy exchanges at the land-atmosphere interface, regardless of the cloud conditions.

## 2. $T_s$ Retrieval Methodology and Evaluation Data Sets

### 2.1. Microwave-Derived $T_s$ Retrievals

#### 2.1.1. Neural Network Retrieval

[6] A Neural Network (NN) inversion scheme with a novel feature of employing a first guess input has been developed by *Aires et al.* [2001] to retrieve simultaneously the land surface  $T_s$ , the atmospheric column water vapor abundance  $WV$ , the cloud liquid water path  $CLW$ , and the surface emissivities,  $ef$ , for all SSM/I channels between 19 and 85 GHz. This NN method optimizes the use of all the SSM/I channels and a priori information to constrain the inversion problem and retrieves simultaneously surface and atmospheric parameters that are consistent among themselves and with the satellite observations.

[7] The database used to train the NN is calculated with a radiative transfer model and a global collection of coincident surface and atmospheric parameters extracted from the National Center for Environmental Prediction (NCEP) [*Kalnay et al.*, 1996], the International Satellite Cloud Climatology Project (ISCCP) cloud parameters and  $T_s$  [*Rossov and Schiffer*, 1999], and pre-calculated monthly-mean land surface emissivities [*Prigent et al.*, 1997, 2006].

[8] To the extent that the training data set provides a realistic joint distribution of the surface and atmospheric parameters, including their correlations, the neural network represents a global statistical fit of the inverse radiative transfer model. The training database is composed of 2 months of global data during 1993 (January and June). The atmospheric relative humidity and temperature are taken from the NCEP reanalysis data set, every 6 h with a spatial resolution of  $2.5^\circ$  in latitude and longitude. The  $WV$  is also used as the first guess a priori information with an assigned error of 40 % of the initial value. This first guess errors is similar to that obtained from the error covariance of each humidity level as given by *Eyre et al.* [1993]. In the ISCCP data set, cloud and surface parameters are retrieved from visible and infrared radiances provided by the set of polar and geostationary meteorological satellites. In this study, the ISCCP data set provides estimates of the cloud-top and surface skin temperatures (<http://isccp.giss.nasa.gov>). The error assigned to the surface temperature values is estimated to be 4 K (see section 2.2.1 below for more details on the ISCCP  $T_s$  estimates). The first guess information for the microwave emissivities at each location is derived from the monthly mean land surface emissivities previously estimated by *Prigent et al.* [1997, 2006]. The standard deviation of day-to-day variations of the retrieved emissivities within a month for each channel and location is used as the estimate of first guess errors. For more information on the a priori first guess information and related background errors, see the work of *Aires et al.* [2001].

[9] To better constrain the problem, the clear/cloudy flag information provided by the ISCCP data set is used to train two neural networks: one for clear scenes and one for cloudy scenes. Both NN retrieve simultaneously  $T_s$ , seven SSM/I  $ef$  and the  $WV$ . For the cloudy NN,  $CLW$  is also retrieved.

Continuity between the NN retrievals at very low  $CLW$  has been verified.

[10] The inversion method provides  $T_s$  for each SSM/I observation over land with a theoretical r.m.s. error of 1.3 K in clear-sky and 1.6 K in cloudy scenes (see *Aires* [2004] and *Aires et al.* [2004a, 2004b] for further analysis of the theoretical inversion errors). *Prigent et al.* [2003a] evaluated the  $T_s$  values with respect to surface air temperature  $T_{air}$  by a comprehensive analysis of the differences expected between the estimated  $T_s$  and the  $T_{air}$  measured at meteorological stations as a function of diurnal and seasonal solar insolation, vegetation cover, and cloudiness variations. The method has also been applied with success over snow and ice [*Prigent et al.*, 2003b].

### 2.1.2. Single Microwave Channel $T_s$ Estimate

[11] The neural network  $T_s$  estimates (hereafter MW1) will be systematically compared to the single channel algorithm (hereafter MW2) developed by *Holmes et al.* [2009]. In MW2, the 37 GHz vertical polarization channel is selected for its low sensitivity to the surface characteristics and relatively high atmospheric transmittance. Over 2005, FLUXNET observations were collected [*Baldocchi et al.*, 2001] and the longwave fluxes were compared to the SSM/I brightness temperatures ( $T_b$ ) at 37 GHz vertical polarization ( $T_b37V$ ), using carefully determined infrared emissivities. A simple linear regression was developed from coincident data at 17 stations in midlatitudes, over a year (2005).  $T_b37V < 259.8$  K were discarded, as they likely represent frozen conditions. In addition, pixels with more than 4% coverage of standing water are excluded as the authors specify that the accuracy of the retrieval is reduced in cases of low emissivity surfaces (the fractional coverage of ocean and permanent inland water bodies is calculated from the International Geosphere-Biosphere Programme (IGBP) one-minute land ecosystem classification map [*Loveland et al.*, 2000]). Radiative transfer simulations were conducted to assess the sensitivity of the retrieval to various parameters (atmospheric water vapor, scattering albedo, roughness, soil moisture, incidence angle, and frequency). The standard deviation of the estimates, as compared to the in situ measurements (not accounted for in the training of the regression but representative of similar environments) is of the order of 2 K for forests and up to 4 K for low density vegetation. The bias was estimated to be within 1 K for most surfaces. The technique is applicable to a large set of microwave imagers (SSM/I, TMI, AMSR-E) all of which provide observations close to 37 GHz in vertical polarization, with an incidence angle around 50°. The authors specify that changes in overpassing time from a satellite to the other and satellite drift can increase the error budget, when calculating long time series.

## 2.2. Evaluation Data Sets

### 2.2.1. Infrared-Derived $T_s$

[12] The ISCCP data set provides the longest satellite  $T_s$  product available today, covering the period from 1983 to present every 3 hours with a spatial sampling interval of 30 km for the full globe under clear-sky conditions (a new version will soon be released with 10 km sampling). Some limitations of this product have been documented [e.g., *Zhang et al.*, 2006] but its potential for climate studies makes it a unique data set. *C. Jiménez et al.* (manuscript in preparation, 2011) also compare the ISCCP  $T_s$  database with other

more recent infrared estimates of  $T_s$ . Note that in the framework of the present work with SSM/I, MODIS estimates would not be usable, due to the mis-match of its overpass time with the SSM/I for a given location. In the ISCCP data, cloud parameters and related quantities are retrieved from visible (VIS  $\sim 0.6 \mu\text{m}$  wavelength) and infrared (IR  $\sim 11 \mu\text{m}$  wavelength) radiances provided by the set of polar and geostationary meteorological satellites [*Rossow and Schiffer*, 1999]. The surface skin temperature is retrieved from clear IR radiances using satellite-derived products to specify the atmospheric temperature and humidity profiles (TIROS Operational Vertical Sounder (TOVS) estimates). *Rossow et al.* [1993] show that the ISCCP sea surface temperatures are in good agreement with other measurements. The local uncertainty of about 2 K combines errors in cloud detection, the satellite radiance calibration, the atmospheric temperature and humidity used in the retrieval, the radiative transfer model treatment of the water vapor absorption, the assumption of unit surface emissivity (instead of roughly 0.98), and the effect of real differences between the skin and bulk surface temperatures. Thus the uncertainties of land surface temperatures associated with these same factors (cloud detection, atmospheric correction, and radiance calibration) are about the same magnitude, 2 K. Two other sources of surface temperature uncertainty that are more important over land are larger and much more rapid temperature variations and larger emissivity variations. *Rossow and Garder* [1993] and *Rossow et al.* [1993] show how the ISCCP algorithm successfully separates these two types of variations and confirm the accuracy of individual surface temperature variations to within about 4 K. In our study, the ISCCP  $T_s$  estimates, initially calculated with unit emissivity, are corrected for the spatial variation of the surface infrared emissivities at  $11 \mu\text{m}$  [*Zhang et al.*, 2010]. The correction is a simple fit to match the radiation calculations. The variation of emissivity depends on surface type, based on the vegetation database from *Matthews* [1983]. The impact of the correction is limited, less than 1 K even over deserts, because the decrease of upward radiance as emissivity decreases is partially offset by increasing reflection of the downwelling radiance from the atmosphere). We estimate that the infrared emissivity variability is equivalent to a spurious temperature variability smaller than 2 K, well within the 4 K uncertainty associated with synoptic variations [*Zhang et al.*, 2006].

### 2.2.2. CEOP Measurements

[13] The CEOP network was designed to provide in situ measurements of meteorological parameters in a variety of environments during the period 2001–2004 (see <http://www.ceop.net/> for more details). Specific references are available for each of the measurement stations. In our study we use the surface skin and air temperature measurements from this network for comparison with the  $T_s$  derived from satellite data. Each data set in the CEOP network has been quality controlled by the provider by documented procedures. We selected only those stations with good enough quality as specified by the providers over the selected year (2003). The uncertainties in the in situ  $T_s$  measurements are not discussed in detail in the CEOP documentations. Major sources of uncertainties are expected to be related to uncertainties in the IR emissivities, to radiometric noise, and to the variability of  $T_s$  during the measurement integration time. From very careful in situ measurements, *Trigo et al.* [2008] estimated an

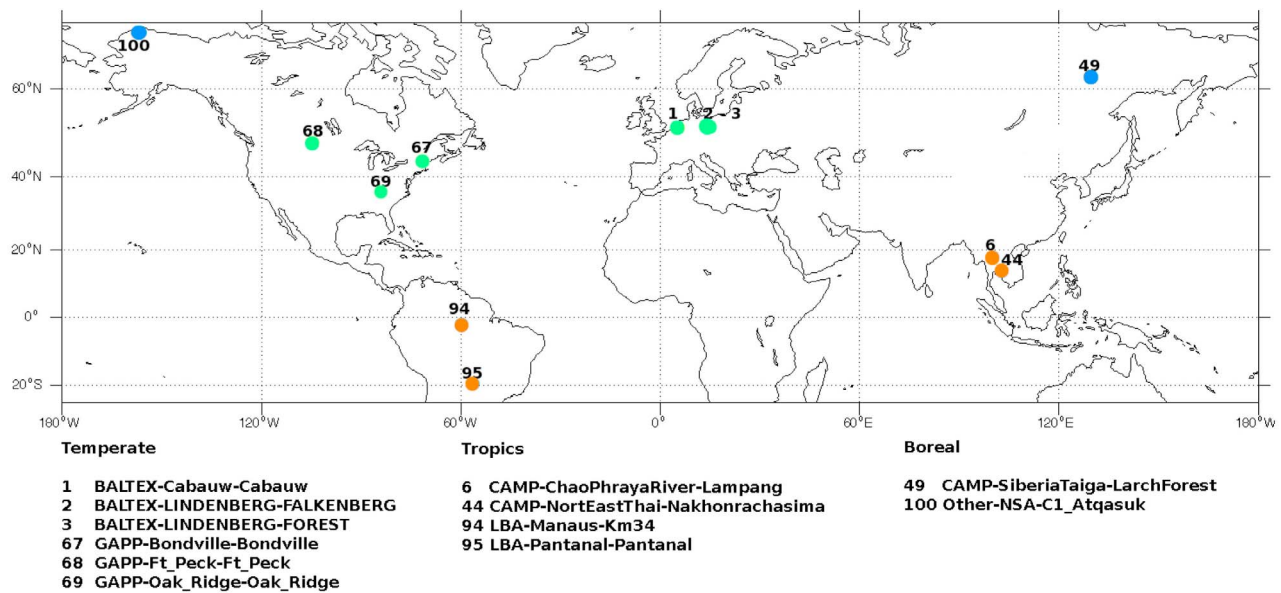


**Figure 1.** Map of the selected CEOP stations. The colors indicate the different environments: green for temperature stations, orange for tropical ones, and blue for the boreal region.

uncertainty of the order of 0.5 K during the night, and up to 1.5 K during the day. The uncertainties in the CEOP measurements are expected to be of the same order. The in situ measurements are matched to the nearest in space and time satellite observations: two measurements are considered coincident when they are within 30 min in time and 25 km in space. Only a limited number of stations in the network provide measurements coincident in time and space with the SSM/I retrievals. For a meaningful comparison of the satellite spatially integrated measurement and the in situ point measurement, stations located in heterogeneous environments are discarded, especially the ones located in coastal regions. Microwave observations are particularly sensitive to the presence of water (the ocean emissivity being much lower than the land emissivity). The presence of the ocean in even a small portion of the field-of-view can significantly impact the observations. Examination of maps (Google Maps) made it possible to filter out the stations located in heterogeneous areas. We also checked the spatial variability of the  $T_s$  IR estimates. The selected stations are grouped into three categories, temperate, tropical, and boreal, to provide a robust and consistent interpretation of the results (see Figure 1).

### 3. Evaluation of the Microwave-Derived $T_s$ Estimates

#### 3.1. Production of the Microwave-Derived $T_s$

[14] The global SSM/I  $T_s$  product has been produced for a 15 year period from 1993 to mid 2008. This involves collecting all SSM/I observations available from the different platforms, along with the ISCCP cloud property and surface temperature data set, and atmospheric properties from the NCEP reanalysis. The products are collocated in space and time and are inputs to the trained neural network inversion process [Aires *et al.*, 2001]. In this study, we concentrate on the evaluation of the  $T_s$  values retrieved in this analysis over the year 2003. To provide a simple reference, the retrieval by

Holmes *et al.* [2009] is also applied for 2003; this method does not require any ancillary data.

[15] At the end of the neural network inversion process, the quality is checked by applying a radiative transfer model to the retrieved parameters ( $T_s$ ,  $ef$ ,  $WV$ , and  $CLW$ ) and comparing the results with the observed brightness temperatures. R.m.s. differences with the input  $Tbs$  are calculated. When this quantity is larger than a threshold corresponding to two standard deviations of the cost function distribution over a full year, the retrieval is labeled as bad. Bad retrievals account for  $\sim 1\%$  and  $\sim 6\%$  of the observations under clear sky and cloudy sky conditions, respectively.  $\sim 61\%$  of the bad cases are related to snow covered surfaces: since the snow emissivity is very variable in space and time, the surface and atmospheric retrieval is particularly difficult [Prigent *et al.*, 2003b; Cordisco *et al.*, 2006]. Unlike the NN method, the Holmes *et al.* [2009] method does not apply to land surfaces with more than 4% of open water, and to frozen or snow covered surfaces. Using the filter for frozen conditions ( $Tb37V < 259.8$  K) suppresses  $\sim 18\%$  (resp.  $\sim 32\%$ ) under clear (resp. cloudy) sky.

#### 3.2. Comparison With Infrared Estimates Under Clear-Sky Conditions

[16] Under clear sky conditions, the microwave retrieval can be compared to the ISCCP collocated estimates obtained from infrared radiances. The overpass times of the SSM/I satellite are around 6:00 in the morning and 18:00 at night. These times correspond to significant changes in  $T_s$  within its diurnal cycle, but the largest variations observed around noon are avoided. Note that in the literature comparisons between  $T_s$  are often limited to nighttime to benefit from more thermal stability. Figure 2 presents maps of monthly mean  $T_s$  for July, calculated for the SSM/I morning overpasses, under clear sky condition only (as specified by the ISCCP cloud flag). The IR estimates and our retrieval present similar  $T_s$  spatial structures. In the Holmes *et al.* [2009]  $T_s$  map,

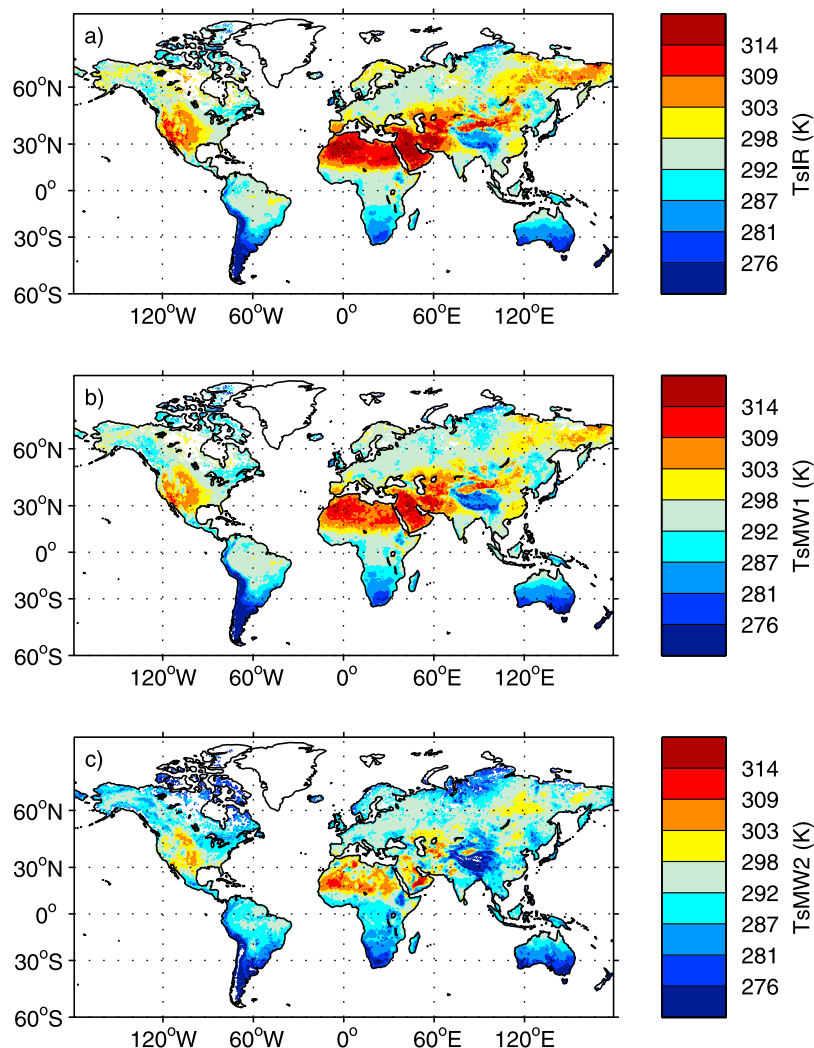


**Figure 2.** Averaged maps of the retrieved  $T_s$  for July morning orbits, for clear pixels (as indicated by the ISCCP cloud flag): (a) from the IR retrieval from ISCCP, (b) from the Neural Network inversion (MW1) [Aires *et al.*, 2001], and (c) from the single frequency method (MW2) [Holmes *et al.*, 2009].

specific patterns appear related more to changes in surface emissivities rather than to real changes in  $T_s$ . This is the case for all unfiltered hydrological structures such as the Amazon River, the Congo River, or the many lakes in Canada: the low emissivity of the standing water induces a decrease of the measured  $T_b$ s at 37 GHz that is confused with a decrease in  $T_s$  in this algorithm, which does not account for surface emissivity changes. By the same token, the carbonate outcrops in Oman or in Egypt that are associated with low emissivities [Prigent *et al.*, 2005; Jiménez *et al.*, 2010] are also falsely interpreted as low  $T_s$ . Figure 3 presents the histograms of the differences under clear sky conditions between the infrared  $T_s$  from ISCCP and the microwave  $T_s$  derived from the NN method (solid line) and the Holmes *et al.* [2009] scheme (dotted line), for January and July. The comparison is limited to the pixels for which both microwave retrievals are valid (as described above). Since the NN method uses the IR  $T_s$  as a priori information, only small biases are expected between the IR  $T_s$  and our microwave estimates. Note nevertheless that the NN methodology has been trained over 2 months

of data in 1993: any changes in the ISCCP methodology or drifts in the different satellite observations (SSM/I and/or IR satellites) can introduce spurious biases. The r.m.s. for January and July are smaller than the r.m.s. differences assigned to the  $T_s$  first guess (4 K). Holmes *et al.* [2009]  $T_s$  shows much more bias: this methodology underestimates  $T_s$  since it was tuned for high emissivities (vegetated areas) and cannot account for lower values. Over snow, the NN method provides a mean difference of  $-1.0$  K and a r.m.s. of 3.5 K in January (the method from Holmes *et al.* [2009] does not provide many estimates over snow because of the threshold on the  $T_b$ s).

[17] In order to further analyze the microwave retrieval under clear condition, the comparison results are separated into microwave emissivity ranges. The microwave emissivity is highly variable in space and time, much more than the infrared emissivity. The lower the emissivity, the lower the contribution from the surface to the radiation (it is proportional to  $ef \times T_s$ ). Table 1 provides the mean and r.m.s. difference between the ISCCP  $T_s$  estimates and the microwave retrievals, when stratified by the microwave

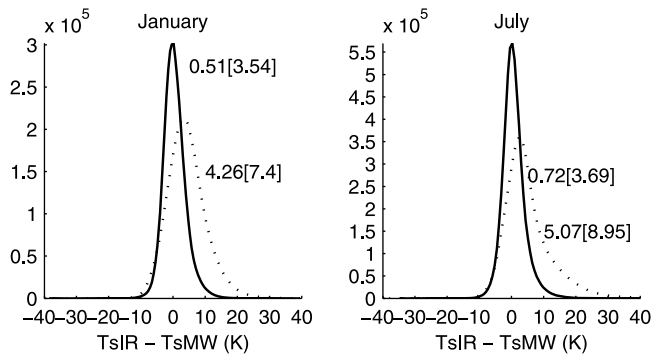


**Figure 3.** For (left) January and (right) July, histograms of the difference under clear sky conditions between the infrared  $T_s$  from ISCCP and the microwave  $T_s$  derived from the NN method MW1 (solid line) and the single frequency scheme MW2 (dotted line). The comparison is limited to the pixels for which both retrievals are valid (condition on the cost function for the first algorithm and threshold on the  $T_b$  at 37 GHz V for the second one, see text). The mean values are indicated, along with the r.m.s. in brackets.

emissivities at 37 GHz vertical polarization. The mean emissivities directly calculated from SSM/I data [Prigent *et al.*, 2006] are used here. Table 1 shows that the NN results are insensitive to changes in surface emissivities with similar performance regardless of the emissivity. This is expected as the emissivity information is accounted for in the retrieval. In contrast, the Holmes *et al.* [2009] retrieval implicitly assumes a constant surface emissivity. As a consequence, varying surface emissivities (due for instance to the presence of soil moisture, standing water, or snow) affect the  $T_s$  retrieval. The land surface emissivities are typically close to 0.95 at 37 GHz vertical polarization and the Holmes *et al.* [2009]  $T_s$  retrieval performs better for high emissivities.

### 3.3. Comparison With the CEOP Measurements

#### 3.3.1. Detailed Analysis of Selected CEOP Stations

[18] Detailed comparisons with the CEOP measurements are made for a few stations representing three very different environments over 2003. The selected stations provide quality measurements for most of the year. The two first stations (stations 2 and 67) are located in the temperate climate zone: station 2 is located in a rural landscape in eastern Germany and station 67 is located in Bondville, Illinois, USA, in corn and soybean crops. Station 44, located in northeast Thailand in a region of manioc fields, represents tropical conditions. Station 100 is representative of the arctic climate and is located in northern Alaska in a tundra environment. Note that this station is in a region of lakes and the Holmes *et al.* [2009] algorithm cannot be applied. Initially, we had also selected stations in Mongolia and Tibet, but found very large discrepancies between these measurements and all satellite estimates. An examination of the spatial variability exhibited by the satellite products suggested a correlation of the large discrepancies and very large spatial heterogeneity as would be expected in elevated, arid environments with significant variations of topographic height. Thus it was not possible to conclude if differences were related to the unrepresentativeness of the in situ

measurements or to limitations of the satellite retrievals in these environments.

[19] Figure 4 shows the time series of the  $T_s$  (Figure 4, left, top panel for each station) and the difference between the satellite estimates and the in situ measurement (Figure 4, left, lower panel for each station). The microwave-derived estimates have the lowest temporal sampling (about two overpasses a day), so the comparisons are limited to the times coincident with the SSM/I microwave observations. The infrared  $T_s$  estimates are available under clear sky condition only, so the statistics are separated into clear and cloudy sky (clear and cloudy  $T_s$  estimates are presented with different symbols in Figure 4, with the cloud flag derived from the ISCCP data set). Figure 4 (right) shows the scatterplots of the estimated  $T_s$  with respect to the in situ measurements. The mean and r.m.s. differences between the  $T_s$  CEOP measurements and the satellite-derived estimates are indicated below each plot, along with the linear correlation coefficient. The Holmes *et al.* [2009] estimates are not available for low  $T_s$  values ( $T_b$  37 GHz below 259.8 K) so the statistical analysis is limited to the situations when the Holmes *et al.* [2009] estimates are available (in the plots the NN retrievals are shown whenever they are available).

[20] The  $T_s$  time series and scatterplots show that the two microwave estimates, clear and cloudy, capture the in situ  $T_s$  variability reasonably well. For stations 2 and 67 (temperate zone) the annual cycle is correctly reproduced (high correlation coefficient between the satellite estimates and the in situ measurements), as well as significant synoptic changes (e.g., the cold air outbreak in mid-March at station 2). At station 44 in the Tropics, the amplitude of the annual cycle is small and, as a consequence, the correlation coefficient tends to be lower. There are notable very large  $T_s$  values reported at CEOP station 44 (in May for instance) that are not reproduced by the satellites (similar situations occur in summer for station 2). Measurements of the surface air temperature are more direct and easier to make than in situ  $T_s$  measurements: the consistency of the  $T_s$  CEOP measurements at station 44 has been evaluated by comparison to the observed surface air temperatures. These large fluctuations observed under cloudy conditions in May for this station do not coincide with comparable changes in surface air temperatures, so they are suspect. For the two temperate stations, the performances of the Holmes *et al.* [2009] algorithm are very different: for instance the bias is  $-1.5$  K under clear conditions at station 2 but  $-5.16$  K at station 67. This behavior is caused by different

**Table 1.** Statistics of the Difference Between the IR and the Microwave Estimates for Different Surfaces, as Separated by Their Microwave Emissivities at 37 GHz Vertical Polarization<sup>a</sup>

	emis37V < 0.90	0.90 < emis37V < 0.95	0.95 < emis37V
	<i>MW1 Retrieval</i>		
January	0.70 (3.52)	0.52 (3.40)	0.47 (3.89)
July	1.75 (4.43)	0.68 (3.54)	0.48 (3.49)
	<i>MW2 Retrieval</i>		
January	14.49 (4.19)	4.52 (3.16)	-1.50 (1.99)
July	17.32 (4.73)	4.45 (3.56)	-1.31 (1.86)

<sup>a</sup>The mean value is indicated as well as the standard deviation into brackets. MW1 indicates the neural network microwave retrieval [Aires *et al.*, 2001], and MW2 the single channel algorithm [Holmes *et al.*, 2009].

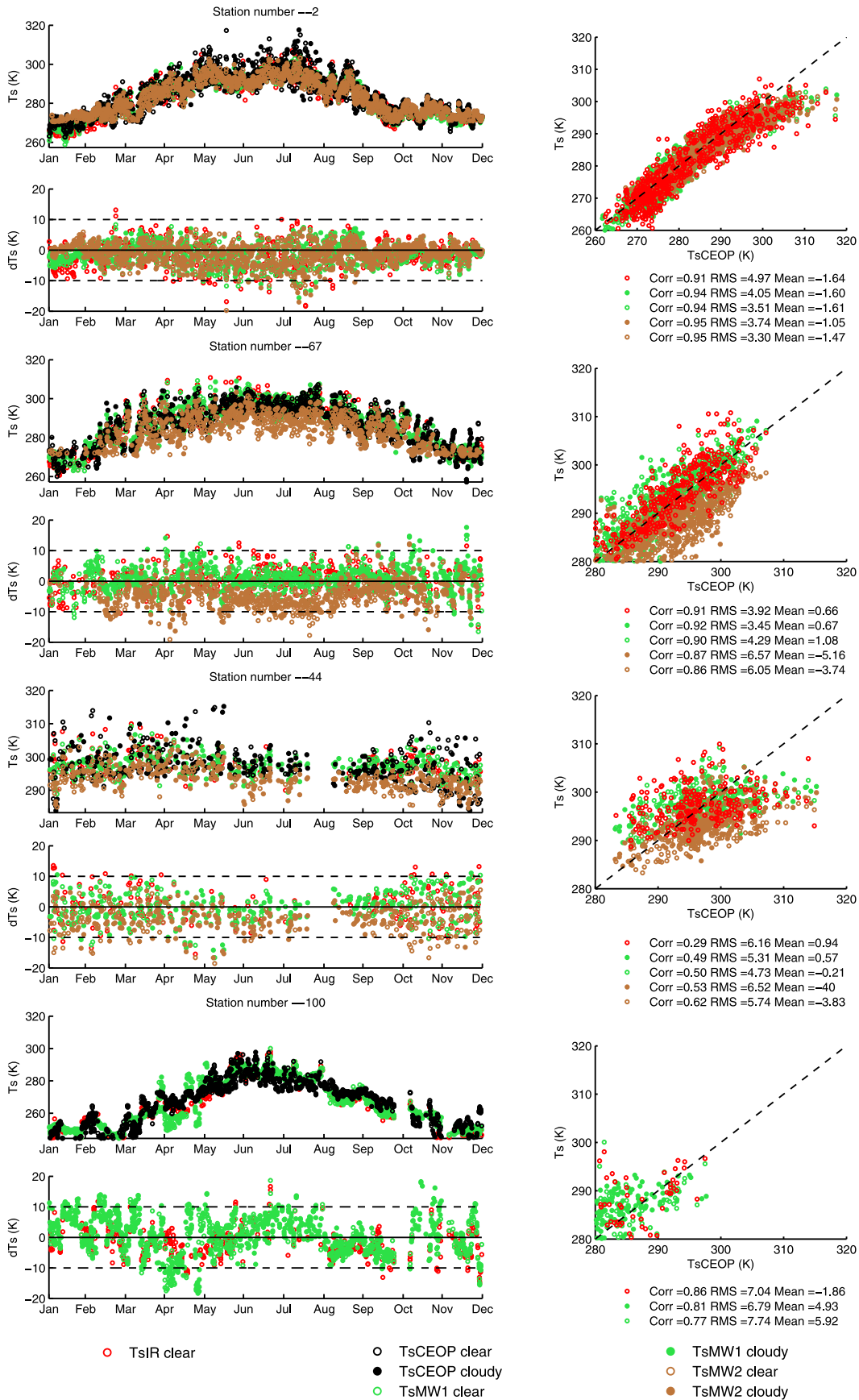


Figure 4

surface emissivities at these two locations, a variable that is not accounted for in this algorithm. Our NN retrieval obtained annual average emissivities at 37 GHz vertical of 0.92 and 0.95 at these two locations, which would explain temperature differences of nearly 6 K. At station 100 (boreal climate) the differences between the in situ and satellite-derived estimates are larger than elsewhere, although the correlation coefficient is still good for our retrieval. The snow and ice emissivities are highly variable in time [Prigent *et al.*, 2003b; Cordisco *et al.*, 2006], and as a consequence, larger errors in the  $T_s$  estimates are expected over these surface types, especially during transition times, when the surface undergoes freezing and thawing cycles.

[21] Regardless of the station, our microwave retrieval performances are similar to the infrared products under clear conditions. In addition, the microwave retrieval approach performs just about as well under cloudy as under clear conditions: the impact of clouds on the microwave measurements is correctly accounted for in the retrievals. This confirms the ability of the microwave observations to provide  $T_s$  estimates, regardless of the cloud conditions.

[22] Figure 5 examines the problem of comparing spatially integrated satellite measurements and in situ point measurements. For two contrasted months (January and July), the difference between the CEOP  $T_s$  measurements and the satellite estimates are plotted, for stations 2 (temperate) and 44 (tropical). The analysis for the other stations showed similar results. Regardless of the satellite estimates, microwave or infrared, the relationship between the two variables shows a linear decrease with increasing CEOP  $T_s$  temperatures. Even larger variations and differences were found for other, less homogeneous locations. Closer examination of this relationship shows that it is related to the averaging effect of the satellite estimates: within a month, the extreme high and low temperatures that are captured by the CEOP in situ measurements are smoothed out within the satellite field-of-view, and, as a consequence, the satellite estimates tend to overestimate (resp. underestimate), the lowest (resp. the highest) values.

[23] As a further evaluation of the satellite estimates, their sensitivity to the water vapor ( $WV$ ) and to the cloud water ( $CLW$ ) is analyzed. Figure 6 shows the difference between the CEOP and satellite  $T_s$ , for stations 2 and 44, first versus the  $WV$  derived from coincident NCEP reanalysis [Kalnay *et al.*, 1996], second versus the  $CLW$  derived from ISCCP [Rossow and Schiffer, 1999]. There is no obvious influence of  $WV$  or  $CLW$  on the  $T_s$  retrieval, regardless of the method (of course, the IR estimates is not considered under cloudy conditions). The lack of sensitivity of the microwave retrieval to the cloud liquid water path is very encouraging, making this technique a powerful complement to the infrared methods under cloudy conditions.

[24] To evaluate the sensitivity of the microwave satellite retrieval to the changes in surface emissivities, we compare differences between the CEOP and satellite  $T_s$  values

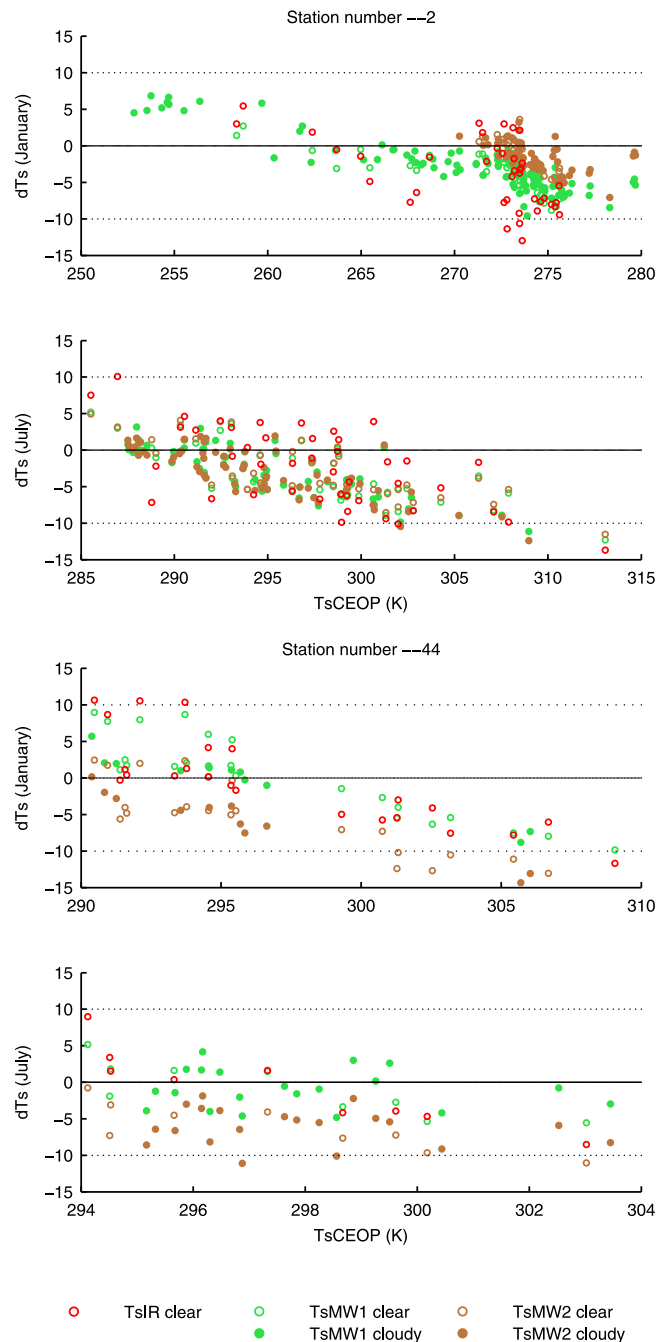


**Figure 5.** Difference between the CEOP and the satellite  $T_s$  versus the CEOP  $T_s$ , for the two selected stations and for two months.

versus the emissivities at 37 GHz (vertical polarization), for all midlatitude stations during 2003 (Figure 7). Here again, it appears that when the emissivity is not taken into account in the retrieval as in the Holmes *et al.* [2009] method, the quality

**Figure 4.** (left) Time series for the selected stations, from top to bottom: two temperature stations (2 and 67), one tropical station (44), and one boreal station (100). For each of the stations, the top plot represents the different LST versus time and the lower one represents the  $T_s$  differences (CEOP  $T_s$  - satellite  $T_s$ ) versus time, for year 2003. (right) Relationship between the satellite-derived  $T_s$  estimates and the CEOP measurements. The linear correlation (C), the r.m.s. of the difference (R), and the mean difference (M), are indicated for each satellite retrieval, separated by clear and cloudy conditions.



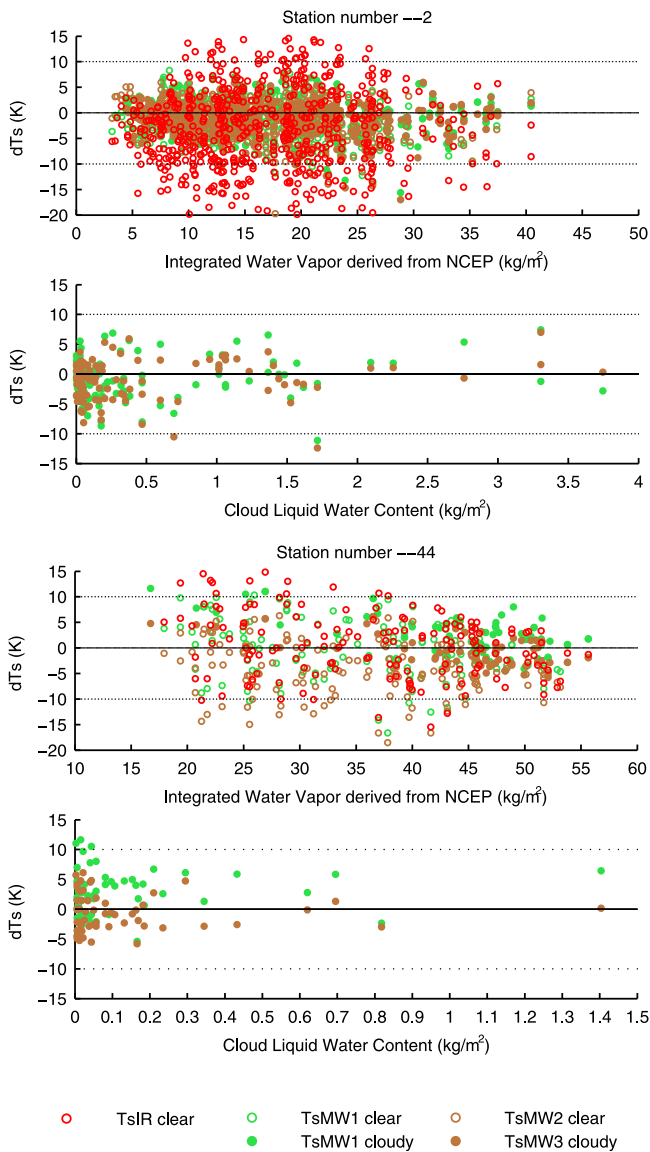


**Figure 6.** For two selected stations, difference between the CEOP and the satellite  $T_s$  versus the water vapor ( $WV$ ) estimated by NCEP (top for each station) and versus the cloud liquid water path ( $CLW$ ) estimated by ISCCP (bottom for each station).

of the microwave estimate of  $T_s$  depends upon the situation, with more errors attached to the situations that are not well captured by the retrieval (the situations of lower emissivities in our case). This confirms what has already been observed in section 3.1. Note nevertheless that a slightly negative slope is also observed for the ISCCP and microwave NN results: It is actually related to the fact that higher emissivities tend to occur for higher temperatures in the data set we have, and larger differences are associated to these situations.

### 3.3.2. Statistical Analysis of the CEOP Data for Different Environments

[25] The previous comparisons are extended to the complete set of selected CEOP stations over a full annual cycle. Table 2 presents the results for each station and each satellite

retrieval. For a specific environment, the results are similar among the stations, except for the *Holmes et al.* [2009] retrieval. To summarize the results, Figure 8 shows the standard deviation of the differences between CEOP and satellite  $T_s$  versus the correlation coefficient for all selected stations, along with the bias. For the IR and NN MW methodologies, the stations located in the temperate region show rather large correlation with small standard deviations and biases. For the microwave retrievals, the results are very similar for both clear and cloudy situations, confirming the role of the microwave estimates to complement the IR methodologies under cloudy conditions.

[26] The r.m.s. differences are typically of the order of 4 K for the midlatitude environment, but can be larger for other environments. Particularly large errors are observed at station 6 in the Tropics, regardless of the satellite method. For this station, we compared the  $T_{air}$  and  $T_s$  in situ measurements, along with the satellite  $T_s$  from different sources under clear sky conditions (ISCCP, MODIS, AIRS) (see C. Jiménez et al., manuscript in preparation, 2011). Both  $T_s$  and  $T_{air}$  are lower during the day than during the night (more than 10 K lower in January) and it seems that the  $T_s$  and  $T_{air}$  variables have been switched because there is good agreement between the satellite  $T_s$  and the in situ  $T_{air}$ , but not with the in situ  $T_s$ . The validity of the in situ measurements at this station is suspect.

[27] For all comparisons, a portion of the error is related to the comparison area-averaged satellite data with in situ point measurements. It has been shown that for a given location, satellite retrieval tends to underestimate the largest  $T_s$  values and to overestimate the smallest  $T_s$  values because of the averaging. The errors that are observed in this study are in line with other results, from independent comparisons involving satellite estimates and in situ measurements. For instance, *Trigo et al.* [2008] compared  $T_s$  derived from the Meteosat Second Generation SEVIRI instrument and in situ measurements under very controlled conditions and found biases up to 2.5 K, during nighttime. At SSM/I overpassing times (around 6:00 and 18:00), insolation can yield large temporal and spatial gradients of  $T_s$ , making it more difficult

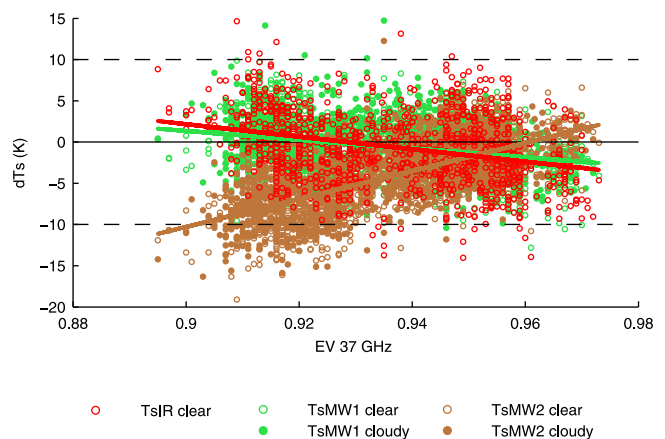


**Figure 7.** For the stations in mid latitude environment (group 2), difference between the CEOP and the satellite  $T_s$  versus the surface microwave emissivity at 37 GHz vertical polarization. The linear fits have been added to the plots.

**Table 2.** Statistics of the Difference Between the Satellite Estimates and the CEOP in Situ Measurements, Over 2003, for All Selected Stations<sup>a</sup>

Region and Station	$T_{IR} - T_{CEOP}$			$T_{MW1} - T_{CEOP}$						$T_{MW2} - T_{CEOP}$					
	Clear			Clear			Cloudy			Clear			Cloudy		
	Mean	RMS	Corr	Mean	RMS	Corr	Mean	RMS	Corr	Mean	RMS	Corr	Mean	RMS	Corr
MidLat															
1	-0.25	4.48	0.81	-0.21	3.73	0.85	-0.55	3.47	0.86	-7.96	8.69	0.87	-8.06	8.51	0.89
2	-1.64	4.97	0.91	-1.60	4.05	0.94	-1.61	3.51	0.94	-1.05	3.74	0.95	-1.47	3.30	0.95
3	-1.46	5.39	0.88	-1.50	4.22	0.93	-1.20	3.75	0.92	-0.89	3.78	0.93	-1.02	3.11	0.93
67	0.66	3.92	0.91	0.67	3.45	0.92	1.08	4.29	0.90	-5.16	6.57	0.87	-3.74	6.05	0.86
68	-1.12	4.89	0.71	-0.20	4.57	0.73	0.45	4.99	0.70	-3.75	6.68	0.54	-2.18	6.00	0.60
69	-2.26	4.97	0.80	-2.04	4.51	0.86	-1.09	3.13	0.88	-4.49	6.23	0.82	-3.37	4.69	0.85
Tropics															
6	-8.54	11.48	0.06	-9.33	11.38	0.28	-8.79	10.53	0.30	-13.42	14.77	0.35	-12.24	13.51	0.29
44	0.94	6.16	0.29	0.57	5.31	0.49	-0.21	4.73	0.50	-4.00	6.52	0.53	-3.83	5.74	0.62
94	-1.97	3.91	0.22	-2.08	3.03	0.64	-2.20	3.09	0.56	-4.92	5.28	0.71	-4.03	4.44	0.64
95	-2.78	6.57	-0.05	-1.64	3.81	0.70	-1.12	3.87	0.62	-1.34	3.32	0.79	-1.45	3.63	0.69
Boreal															
49	-6.46	9.11	0.74	-3.49	6.40	0.82	0.05	4.68	0.85						
100	-1.86	7.04	0.86	4.93	6.79	0.81	5.92	7.74	0.77						

<sup>a</sup>The mean, the r.m.s. and the correlation coefficient are indicated, separately for clear and cloudy situations, respectively for the IR ISCCP estimates, for the NN microwave retrieval (MW1), and for the single channel microwave retrieval (MW2). For the Boreal stations, MW2 cannot be applied as the pixels have more than 4% water coverage.

to compare in situ and satellite observations that are not exactly coincident in time and space.

**4. Conclusion**

[28] Microwave satellite estimates of surface skin temperature are carefully evaluated through comparisons with in situ CEOP measurements in different environments that include temperate, tropical, and boreal regions, over a full annual cycle (2003). In addition, the IR ISCCP  $T_s$  are also examined and compared to the other measurements. Comparison between satellite observations over extended pixels and in situ point measurements is always challenging and requires great care. In this exercise, we select in situ stations that are located in homogeneous environments and that provide a significant amount of data all year long. A total of twelve stations are analyzed.

[29] Under clear sky conditions, the quality of our microwave neural network retrieval is equivalent to the IR ISCCP products, for most stations. For a given location, the performance of the microwave algorithm is similar under clear and cloudy conditions, confirming that our retrieval has accounted for the limited effect of the clouds. A simpler approach, the *Holmes et al.* [2009] algorithm also yields realistic estimates of  $T_s$ , when the surface emissivity at 37 GHz (vertical polarization) is similar to that for the locations used to test the algorithm, i. e., near unity. In these regions, this simple algorithm can provide a  $T_s$  first guess that could be further refined in a more complex algorithm, such as in our NN methodology.

[30] Our microwave  $T_s$  estimates have been calculated for more than 15 years (1993 to mid 2008), from all available SSM/I observations. The same methodology could be applied to AMSR-E measurements. These “all weather”  $T_s$  estimates are a very valuable complement to the IR-derived  $T_s$ , for use in atmospheric and surface models.

[31] However, the accuracy of the products has to be carefully considered, especially when used to calculate

radiative and turbulent fluxes. The longwave fluxes at the surface vary by about  $7 \text{ W.m}^{-2}$  for every degree of temperature [*Zhang et al.*, 1995]. For sensible flux estimation, the key variable is the difference between  $T_s$  and  $T_{air}$  and the uncertainty in one estimate can result in large errors in the fluxes. One of the objectives of the GEWEX LandFlux program [e.g., *Jiménez et al.*, 2010] is to determine the

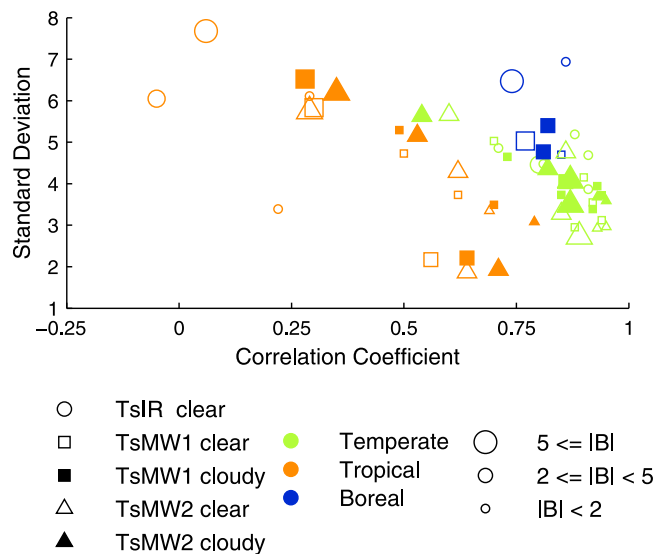


**Figure 8.** Scatterplot of the standard deviation of the difference between CEOP and satellite  $T_s$  versus the correlation coefficient between the two variables, for each selected stations. Symbols (circles, squares, and triangles) indicate the considered satellite product. Empty symbols indicate clear sky conditions and filled symbols indicate cloudy conditions. The color of the symbols is representative of the station group (see Figure 1). The size of each symbol gives an idea of the bias (in absolute value).

potential for estimating the turbulent fluxes, given the available input data, including  $T_s$ , and to guide development of better products.

[32] **Acknowledgments.** The authors wish to thank Thomas Holmes and Tom Jackson for their careful reading of the manuscript and their very valuable comments. They are also thankful to three anonymous reviewers for their careful reading and interesting suggestions. Work on this study by Catherinot and Rossow was supported by NASA grant NNXD7A090G, the NASA Energy and Water Study (NEWS).

## References

- Aires, F. (2004), Neural network uncertainty assessment using Bayesian statistics with application to remote sensing: 1. Network weights, *J. Geophys. Res.*, *109*, D10303, doi:10.1029/2003JD004173.
- Aires, F., C. Prigent, W. B. Rossow, and M. Rothstein (2001), A new neural network approach including first guess for retrieval of atmospheric water vapor, cloud liquid water path, surface temperature, and emissivities over land from satellite microwave observations, *J. Geophys. Res.*, *106*, 14,887–14,907.
- Aires, F., C. Prigent, and W. B. Rossow (2004a), Neural network uncertainty assessment using Bayesian statistics with application to remote sensing: 2. Output errors, *J. Geophys. Res.*, *109*, D10304, doi:10.1029/2003JD004174.
- Aires, F., C. Prigent, and W. B. Rossow (2004b), Neural network uncertainty assessment using Bayesian statistics with application to remote sensing: 3. Network Jacobians, *J. Geophys. Res.*, *109*, D10305, doi:10.1029/2003JD004175.
- Baldocchi, D., et al. (2001), FLUXNET: A new tool to study the temporal and spatial variability of ecosystem-scale carbon dioxide, water vapor, and energy flux densities, *Bull. Am. Meteorol. Soc.*, *82*, 2415–2434.
- Basist, A., N. C. Grody, T. C. Peterson, and C. N. Williams (1998), Using the Special Sensor Microwave/Imager to monitor land surface temperatures, wetness, and snow cover, *J. Atmos. Sci.*, *37*, 888–911.
- Cordisco, E., C. Prigent, and F. Aires (2006), Snow characterization at a global scale with passive microwave satellite observations, *J. Geophys. Res.*, *111*, D19102, doi:10.1029/2005JD006773.
- Eyre, J. R., G. A. Kelly, A. P. McNally, E. Andersson, and A. Persson (1993), Assimilation of TOVS radiance information through one-dimensional variational analysis, *Q. J. R. Meteorol. Soc.*, *119*, 1427–1463.
- Holmes, T. R. H., R. A. M. De Jeu, M. Owe, and A. J. Dolman (2009), Land surface temperature from Ka band (37 GHz) passive microwave observations, *J. Geophys. Res.*, *114*, D04113, doi:10.1029/2008JD010257.
- Jiménez, C., J. Catherinot, C. Prigent, and J. Roger (2010), Relations between geological characteristics and satellite-derived infrared and microwave emissivities over deserts in northern Africa and the Arabian Peninsula, *J. Geophys. Res.*, *115*, D20311, doi:10.1029/2010JD013959.
- Jones, L. A., C. R. Ferguson, J. S. Kimball, K. Zhang, S. T. K. Chan, K. C. McDonald, E. G. Njoku, and E. Wood (2010), Satellite microwave remote sensing of daily land surface air temperature minima and maxima from AMSR-E, *IEEE J. Sel. Top. Appl. Earth Obs. Remote Sens.*, *3*, 111–123.
- Kalnay, E., et al. (1996), The NCEP/NCAR 40-year reanalysis project, *Bull. Am. Meteorol. Soc.*, *77*, 437–470.
- Loveland, T. R., B. C. Reed, J. F. Brown, D. O. Ohlen, J. Zhu, L. Yang, and J. W. Merchant (2000), Development of a global land cover characteristics database and IGBP DISCover from 1 km AVHRR data, *Int. J. Remote Sens.*, *21*, 1303–1330.
- MacFarland, J. M., R. L. Miller, and C. M. U. Neale (1990), Land surface temperature derived from the SSM/I passive microwave brightness temperatures, *IEEE Trans. Geosci. Remote Sens.*, *28*, 839–845.
- Matthews, E. (1983), Global vegetation and land use: New high-resolution data bases for climate studies, *J. Clim. Appl. Meteorol.*, *22*, 474–486.
- Njoku, E. G. (1995), Surface temperature estimation over land using satellite microwave radiometry, in *Passive Microwave Remote Sensing of Land-Atmosphere Interaction*, edited by B. J. Choudhury et al., pp. 509–530, VSP, Utrecht, Netherlands.
- Prata, A. (1993), Land surface temperatures derived from the advanced very high resolution radiometer and the along-track scanning radiometer: 1. Theory, *J. Geophys. Res.*, *98*, 16,689–16,702.
- Prata, A. (1994), Land surface temperatures derived from the advanced very high resolution radiometer and the along-track scanning radiometer: 2. Experimental results and validation of AVHRR algorithms, *J. Geophys. Res.*, *99*, 13,025–13,058.
- Prigent, C., W. B. Rossow, and E. Matthews (1997), Microwave land surface emissivities estimated from SSM/I observations, *J. Geophys. Res.*, *102*, 21,867–21,890.
- Prigent, C., F. Aires, and W. B. Rossow (2003a), Land surface skin temperatures from a combined analysis of microwave and infrared satellite observations for an all-weather evaluation of the differences between air and skin temperatures, *J. Geophys. Res.*, *108*(D10), 4310, doi:10.1029/2002JD002301.
- Prigent, C., F. Aires, and W. B. Rossow (2003b), Retrieval of surface and atmospheric geophysical variables over snow-covered land from combined microwave and infrared satellite observations, *J. Appl. Meteorol.*, *42*, 368–380, doi:10.1175/1520-0450(2003)042<0368:ROSAAG>2.0.CO;2.
- Prigent, C., J. Munier, B. Thomas, and G. Ruffié (2005), Microwave signatures over carbonate sedimentary platforms in arid areas: Potential geological applications of passive microwave observations?, *Geophys. Res. Lett.*, *32*, L23405, doi:10.1029/2005GL024691.
- Prigent, C., F. Aires, and W. B. Rossow (2006), Land surface microwave emissivities over the globe for a decade, *Bull. Am. Meteorol. Soc.*, *87*, 1573–1584, doi:10.1175/BAMS-87-11-1573.
- Rossow, W. B., and L. C. Garder (1993), Validation of ISCCP cloud detections, *J. Clim.*, *6*, 2370–2393.
- Rossow, W. B., and R. A. Schiffer (1999), Advances in understanding clouds from ISCCP, *Bull. Am. Meteorol. Soc.*, *80*, 2261–2288, doi:10.1175/1520-0477(1999)080<2261:AIUCFI>2.0.CO;2.
- Rossow, W. B., A. W. Walker, and L. C. Garder (1993), Comparison of ISCCP and other cloud amounts, *J. Clim.*, *6*, 2394–2418, doi:10.1175/1520-0442(1993)006<2394:COIAOC>2.0.CO;2.
- Royer, A., and S. Poirier (2010), Surface temperature spatial and temporal variations in North America from homogenized satellite SMMR-SSM/I microwave measurements and reanalysis for 1979–2008, *J. Geophys. Res.*, *115*, D08110, doi:10.1029/2009JD012760.
- Trigo, I. F., I. T. Monteiro, F. Olesen, and E. Kabsch (2008), An assessment of remotely sensed land surface temperature, *J. Geophys. Res.*, *113*, D17108, doi:10.1029/2008JD010035.
- Wen, J., Z. Su, and Y. Ma (2003), Determination of land surface temperature and soil moisture from Tropical Rainfall Measuring Mission/Microwave Imager remote sensing data, *J. Geophys. Res.*, *108*(D2), 4038, doi:10.1029/2002JD002176.
- Weng, F., and N. C. Grody (1998), Physical retrieval of land surface temperature using the special sensor microwave imager, *J. Geophys. Res.*, *103*, 8839–8848.
- Williams, C. N., A. Basist, T. C. Peterson, and N. Grody (2000), Calibration and verification of land surface temperature anomalies derived from the SSM/I, *Bull. Am. Meteorol. Soc.*, *81*, 2141–2156.
- Zhang, Y.-C., W. B. Rossow, and A. A. Laci (1995), Calculation of surface and top-of-atmosphere radiative fluxes from physical quantities based on ISCCP data sets: 1. Methods and sensitivity to input data uncertainties, *J. Geophys. Res.*, *100*, 1149–1165, doi:10.1029/94JD02747.
- Zhang, Y.-C., W. B. Rossow, and P. W. Stackhouse Jr. (2006), Comparison of different global information sources used in surface radiative flux calculation: Radiative properties of the near-surface atmosphere, *J. Geophys. Res.*, *111*, D13106, doi:10.1029/2005JD006873.
- Zhang, Y.-C., C. N. Long, W. B. Rossow, and E. G. Dutton (2010), Exploiting diurnal variations to evaluate the ISCCP-FD flux calculations and radiative-flux-analysis-processed surface observations from BSRN, ARM, and SURFRAD, *J. Geophys. Res.*, *115*, D15105, doi:10.1029/2009JD012743.

F. Aires, Estellus, 93 Boulevard de Sébastopol, F-75002 Paris, France.  
J. Catherinot, C. Jiménez, and C. Prigent, Laboratoire d'Etudes du Rayonnement et de la Matière en Astrophysique, Observatoire de Paris, CNRS, F-75014 Paris, France. (catherine.prigent@obspm.fr)

R. Maurer, NASA Goddard Institute for Space Studies, Columbia University, 2880 Broadway, New York, NY 10025, USA.

F. Papa, Laboratoire d'Etudes en Géophysique et Océanographie Spatiales, IRD, 18 Avenue Edouard Belin, F-31400 Toulouse, France.

W. B. Rossow, NOAA Cooperative Remote Sensing Science and Technology Center, City College of New York, New York, NY 10031, USA.